# Alteration Products of Uraninite from the Colorado Plateau

**Donggao Zhao and Rodney C. Ewing***

Department of Nuclear Engineering and Radiological Sciences
Department of Geological Sciences
University of Michigan, Ann Arbor, Michigan 48109-2104

* Corresponding author, tel. (734) 647-8529, fax (734) 647-8531, email: rodewing@umich.edu

February 21, 2000

---

Submitted to *Radiochimica Acta* and presented at the Seventh International Conference on the Chemistry and Migration Behavior of Actinides and Fission Products in the Geosphere (Migration '99)

**Alteration Products of Uraninite from the Colorado Plateau**

**Donggao Zhao and Rodney C. Ewing***

Department of Nuclear Engineering and Radiological Sciences
Department of Geological Sciences
University of Michigan, Ann Arbor, Michigan 48109-2104

## Summary

Uraninite and associated alteration products from the Colorado Plateau were studied by optical microscopy, electron microprobe analysis (EMPA), scanning electron microscopy (SEM) and backscattered electron (BSE) imaging in order to determine the behavior and fate of trace elements, such as Pb, Ca, Si, Th, Zr, and REE, during corrosion under oxidizing conditions. The long-term alteration products and processes of uraninite may provide insight into the corrosion of the $UO_2$ in spent nuclear fuel. Uraninite, schoepite, calciouranoite, uranophane, fourmarierite, a Fe-rich uranyl phase, and coffinite were identified. The primary uraninites and alteration phases generally have low trace element contents, except for coffinite from Caribou Mine, Colorado that has $Y_2O_3$ as high as 0.88 wt %. The highest Zr, Ti, Th and REE values of the uraninite are $ThO_2$ 0.17, $Y_2O_3$ 0.28, $La_2O_3$ 0.03, $Ce_2O_3$ 0.10, $Pr_2O_3$ 0.02, $Nd_2O_3$ 0.14, $Sm_2O_3$ 0.12, $Eu_2O_3$ 0.04, $Gd_2O_3$ 0.08, $ZrO_2$ 0.93, and $TiO_2$ 0.54 wt %, which are in general lower than the corresponding components in secondary uranyl phases (the highest values are $ThO_2$ 0.21, $Y_2O_3$ 0.88, $La_2O_3$ 0.05, $Ce_2O_3$ 0.15, $Pr_2O_3$ 0.05, $Nd_2O_3$ 0.18, $Sm_2O_3$ 0.14, $Eu_2O_3$ 0.11, $Gd_2O_3$ 0.08, $ZrO_2$ 2.11, and $TiO_2$ 2.74 wt %), suggesting that trace elements preferentially enter the structures of these secondary uranyl phases (Table 2). A compositional profile of a concentric structure in schoepite shows that, with increasing alteration, $UO_2$, PbO and $ZrO_2$ decrease, and $SiO_2$, $TiO_2$, CaO and $P_2O_5$ increase. Alteration causes loss of U, Pb and Zr and incorporation of Si, Ti, Ca and P into

* Corresponding author, tel (734) 647-8529, fax (734) 647-8531, email: rodewing@umich.edu

uranyl phases. The Ca-rich calciouranoite from Grants, New Mexico, indicates an interaction between the limestone host rock and uranium minerals. Texturally, concentric structures and micro-fractures are common. Concentric structures are usually composed of both uraninite and uranyl phases, while micro-fractures are common in the secondary phases.

KEYWORDS: URANINITE, ALTERATION, SCHOEPITE, CALCIOURANOITE, URANOPHANE, FOURMARIERITE, SPENT FUEL, URANYL PHASES

## Introduction

A significant proportion of the radioactivity in spent nuclear fuel is associated with trace elements (~ 4 % fission products and actinides) in the $UO_2$ [1]. Under oxidizing conditions, the $UO_2$ in spent nuclear fuel is not stable; uranium is up to four orders of magnitude more soluble than under reducing conditions [2-3]. Therefore, uranium tends to leach from surface disposal sites, move with groundwater, and concentrate where reducing environments prevail. The fate of radionuclides released from spent nuclear fuel is a critical aspect of the performance assessment of a spent fuel repository under oxidizing conditions. The radionuclides released during the corrosion of $UO_2$ may, however, become incorporated into the structures of the secondary uranyl phases formed [4-5]. Natural uraninite $UO_{2+x}$ and its alteration products can be used to investigate trace element incorporation into these secondary alteration phases [6-10]. Investigation of natural uraninites and the migration and fate of impurity components has, therefore, attracted much attention in recent years [e.g., 11-15].

Characterization of natural uraninites and its alteration products has required the use of a variety of analytical techniques, for example, optical microscopy [2], scanning electron microscopy (SEM) [16-17], electron microprobe analysis (EMPA) [16, 18, 12, 19-23], X-ray diffraction (XRD) [17], X-ray photoelectron spectroscopy (XPS) [17, 24], neutron activation analysis (NAA) [25], proton probe analysis or particle-induced X-ray emission (PIXE) [16],

secondary ion mass spectrometry (SIMS) [26], induced coupled plasma atomic emission spectroscopy (ICP-AES) [24]. However, there are only a few studies of uraninite and associated alteration products by EMPA. Previous EMPA studies include uraninite in sandstones from the southwestern part of the former Yugoslavia [16], uraninite in dolostones or siltstones from the Shinkolobwe, Katanga, former Zaire [18], uraninite from the natural fission reactors and uranium ore at Oklo, Okélobondo, and Bangombé in Gabon, West Africa [12, 19, 23], uraninite in the Ruggles and Palermo granitic pegmatite, Grafton County, New Hampshire [21], and uraninite in granites from Erzgebirge, Germany/Czech Republic [22]. In a study of the alteration products of natural uraninite and chemical variations and trace element contents of uraninite and its alteration products, we have primarily employed EMPA to study uraninites from the Colorado Plateau in the western United States. The main aim of this paper is to decide the corrosion products of uraninite, the migration and fate of trace and minor elements during the alteration of uraninite, and the interaction of uranium minerals with country rocks and ground waters under oxidizing conditions.

**Analytical methods**

Chemical compositions of natural uraninite $UO_{2+x}$ and its alteration products were determined by EMPA on a Cameca CAMEBAX electron microprobe (wavelength dispersive spectrum or WDS) at the University of Michigan Electron Microbeam Analysis Laboratory. The Cameca PAP correction routine $\phi(\rho z)$, i.e., modified ZAF by Pichou and Pichouir [27], was used in data reduction. Samples were usually analyzed by using a rastered beam (3x3 $\mu m^2$) at an accelerating voltage of 20 kV in order to avoid damage to uranyl phases by electron beam. If there was no significant amounts of volatile components, such as $H_2O$, the phase is analyzed by a focused beam in spot mode. We have focused on the analysis of Th and rare earth elements (REE), besides common elements in uraninite and its alteration products, such as U, Pb, Si, and Ca. Twenty-four elements are included in the analytical procedure (Table 1). To increase

counts, a beam current of 80 nA was used for Pb, U and Th. For other elements a beam current of 20 nA was used. Peak count time was 30 seconds. $M_\beta$ line was used for U to avoid interference from Th $L_\gamma$, Zr $K_\alpha$, Fe $K_\alpha$ and Pb $L_\beta$ lines. $K_\alpha$ lines were used for Si, Ca, P, Mg, Al, K, Na, Mn, Ti, Fe, and S; $L_\alpha$ lines for Y, La, Ce, Pr, Nd, Sm, Eu, Gd, Sr and Zr; and $M_\alpha$ lines for Th and Pb. Oxygen was obtained by stoichiometry. The detailed procedure (elements analyzed, standards, characteristic X-ray line, beam current and voltage) is summarized in Table 1.

Back scattered electron imaging was used to characterize textural and mineralogical features of the samples. Energy dispersive spectrum (EDS) analysis was used to qualitatively determine the elemental distribution. Both BSE images and EDS spectra were obtained from a Hitachi S3200N scanning electron microscope.

**Samples and petrography**

There are three major origins of natural uraninites, i.e., pegmatitic (igneous), vein-type (hydrothermal) and sedimentary (low temperature) [2]. Pegmatitic uraninite usually contains high amounts of impurity components (mainly Th and REE); hydrothermal uraninites have minor amounts of Y, REE, Ca and/or Th; and sedimentary uraninites may contain abundant Ca, Si and P [2]. There are a number of small uranium deposits on the Colorado Plateau that are sedimentary or hydrothermal or both in origin and occur largely in sandstones or as veins [28-29]. Uranium deposits in sandstones are predominantly tabular approximately parallel to the bedding of the sedimentary host rock [28, 30]. The most favorable host rock is impure medium- to coarse-grained quartz sandstones or conglomerates. The uranium minerals occur interstitially, filling pore spaces rather than forming continuous deposits [30]. Some of these deposits, e.g., those near Marysvale, Piute County, Utah [31] and from Central City District, Gilpin County, Colorado [32], have uraninites with high impurity contents. In terms of conditions of alteration, these localities have much in common with Yucca Mountain, Nevada, that is a relatively arid environment. The samples studied are from Caribou Mine, Boulder County, Colorado; Jefferson

County, Colorado; Marshall Pass District, Saguache County, Colorado; Happy Jack Mine, White Canyon, near Blanding, Utah; and Grants, New Mexico (Fig. 1). These samples were selected for the following reasons: 1) Uranium mineralization is young and radiogenic Pb-content is low [29], mostly from Late Cretaceous-Early Tertiary to Late Tertiary (73 to 2 million years in age [33-34]). 2) Strong alteration has occurred since the uranium mineralization. 3) A variety of uranyl phases were identified, providing a unique opportunity to study the migration and partitioning of elements between different uranium phases.

Uranium ore veins from the Caribou Mine, Boulder County, Colorado occur mainly in the monzonite of the Caribou stock, which intruded into Precambrian biotite gneiss. The monzonite host is Late Cretaceous or Tertiary in age; the uranium mineralization is thought to be Tertiary (65 to 2 million years [29]). The common gangue minerals are quartz, dolomite and calcite. Sulfides identified by BSE and EDS include galena PbS, chalcopyrite $CuFeS_2$, tetrahedrite $(Cu,Fe)_{12}Sb_4S_{13}$, and a Pb+Ag sulfide (sample # 603). The galena is subhedral or anhedral and closely associated with uranium minerals (Fig. 2A). In addition, gold, silver, hematite $Fe_2O_3$, sphalerite ZnS, gersdorffite NiAsS, argentite $Ag_2S$, and proustite $Ag_3AsS_3$ were reported [29].

The country rock of uranium ore veins from Jefferson County, Colorado is Precambrian, consisting of complexly folded and faulted metasedimentary rocks. The U-Pb age of a uranium ore from this location is 69 million years [35]. The common gangue minerals are ankerite, quartz, and calcite [29]. Besides uranium minerals, phases identified in uranium ore include trace amounts of sphalerite, pyrite, chalcocite $Cu_2S$ or covellite CuS, and K-feldspar (sample # 637). In hand specimen, the ores have been altered to yellow uranyl phases. BSE images (Fig. 2B and 2C) show that concentric bands are common and different uranium minerals coexist, providing a good opportunity to examine migration of elements among different phases.

Uranium mineralization of the Marshall Pass District, Saguache County, Colorado, occurs in fault-controlled veins and breccia zones in limestone of the Pennsylvanian Belden Formation (approximately 320 to 300 million years) [29]. The uranium ore is located at the intersection of major faults with Tertiary (65 to 2 million years) erosion surfaces. These surfaces

were buried by Early Tertiary siliceous tuffs - a likely source of the uranium [36]. The main uranium mineral is uraninite; traces of sulfides also occur. Concentric bands (Fig. 2D) are also common (sample # 530 and # 531).

Uraninite from the Happy Jack Mine, White Canyon, southeastern Utah is 65 million years of age [30]. The anhedral uraninites occur in quartz sandstone and are usually distributed along the bedding of quartz grains (sample # 386, Fig. 2E). The uraninites vary from a few microns to up to a few millimeters in size. The major mineral of the host rock is quartz (up to 90 %). Minor minerals are sulfides and some K-feldspar in the interstices of quartz grains. These sulfides include chalcopyrite, $CuFeS_2$, and galena, PbS, as inclusions in chalcopyrite, sphalerite ZnS, pyrite $FeS_2$, and a Co+Ni sulfide as euhedral inclusions in uraninite.

The uranium ore from the Grants uranium region, New Mexico (the southeastern Colorado Plateau) occurs in limestone. The mineralization from this region is primarily of the sandstone type in which the uranium is associated with redistributed carbonaceous materials. Primary mineralization is at least 140 to 130 million years old, followed by a remobilization event at 115 to 110 million years with the formation of a roll-type deposit. Redistributed ore associated with oxidizing alteration (hematization and limonitization) has apparent ages of 3 to 13 million years [37-38]. Pyrite was identified and euhedral galena crystals occur as inclusions in uranium minerals (sample 369, Fig. 2F).

**Results and discussion**

Average electron microprobe analyses of the uranium phases, together with the calculated formula, are given in Table 2. Uranium minerals can be divided into different types based on their chemical compositions. The common types are $U^{4+}$ minerals (e.g., coffinite $U(SiO_4)_{1-x}(OH)_{4x}$), $U^{4+}$-$U^{6+}$ minerals (e.g., uraninite $UO_{2+x}$ and ianthinite $UO_2 \cdot 5UO_3 \cdot 10H_2O$), uranyl oxide hydrates (e.g., schoepite $[(UO_2)_8O_2(OH)_{12}](H_2O)_{12}$ [39]), alkali and alkaline-earth uranyl oxide hydrates (e.g., fourmarierite $PbU_4O_{13} \cdot 6H_2O$), uranyl silicates (e.g., soddyite $(UO_2)_2SiO_4 \cdot 2H_2O$

and uranophane $Ca(UO_2)_2Si_2O_7{\cdot}6H_2O$), and uranyl phosphates [37]. Unlike the $UO_2$ in spent nuclear fuel, natural uraninite commonly contains $U^{4+}$ and $U^{6+}$. Uranium from EMPA must be recalculated into $U^{4+}$ and $U^{6+}$. Therefore, formula of naturally occurring uraninite can be expressed as $UO_{2+x}$, where x is the amount of $U^{4+}$ converted to or replaced by $U^{6+}$ ($UO_{2+x}$ is still stoichiometric, but with a different ratio of $U^{4+}$:$U^{6+}$). Impurities in uraninite include Si, Zr, Th, Y, REE, and radiogenic Pb. Thus, a more detailed structural formula for natural uraninite can be written as $[U^{4+}_{1-x-y-z-u}U^{6+}_x(Th^{4+})_uREE^{3+}_yM^{2+}_z]O_{2+x-(0.5y)-z}$ [40]. Possible presence of $H_2O$ and $CO_2$ in uranyl phases makes the formula calculation of these phases problematic. The following procedure was used when calculating chemical formula from EMPA: 1) lead is assumed to be radiogenic and PbO is recalculated to $UO_2$; 2) if after converting PbO to $UO_2$, the EMPA total is less than 100 wt %, $U^{4+}$ is converted to $U^{6+}$, adding one oxygen per U atom; 3) if all $U^{4+}$ is converted to $U^{6+}$ and the total is still less than 100 wt %, then $H_2O$ and $CO_2$ may exist in the phase; 4) if all $U^{4+}$ is converted to $U^{6+}$ and the total is more than 100 wt %, then only part of $U^{4+}$ can be converted to $U^{6+}$, thus suggesting a $U^{4+}$-$U^{6+}$ phase. For the purpose of comparison, in Table 2, formulae of uranium minerals were normalized to one cation, and volatile components, such as $H_2O$ and $CO_2$, were not included. Σ1 is the sum of all oxides from EMPA, Σ2 is the total after PbO is converted to $UO_2$, Σ3 is the total after $UO_2$ is recalculated to $UO_2$ and $UO_3$.

*Uraninite*

Uraninite was identified in samples from the Marshall Pass District, Saguache County, Colorado (samples # 530 and # 531) and the Happy Jack Mine, near Blanding, Utah (samples # 386 and # 393). The uraninites from the Marshall Pass District have high $U^{6+}$ content (0.587 to 0.808 atom per formula unit or apfu), thus a high total oxygen (2.480 to 2.727 apfu) in the calculated formula according to the above criteria (Table 2), close or similar to altered secondary uraninite, which generally has a stoichiometry of $U_3O_8$ [41-42]. One sample (# 531) has massive uraninite with a schoepite rim surrounded by a late stage uraninite crust. Lead content varies from 2.51 wt % PbO in the central part of the structure to 1.53 wt % in the bright crust. $UO_2$ plus

converted radiogenic Pb of the uraninite from the Marshall Pass District is relatively constant, between 90.99 and 92.25 wt %. The uraninites have incorporated minor Ca, Zr, Ti, Fe, Si and P. Elements such as Th and REE are low or below detection limits, e.g., $ThO_2$ from 0.04 to 0.17, and $Y_2O_3$ from 0.09 to 0.14 (Table 2).

In contrast, the uraninites from the Happy Jack Mine, Utah, have a low $U^{6+}$ content (0.212 to 0.489 apfu) and low total oxygen (2.107 to 2.354 apfu) in the calculated formula (Table 2), close to that of an unaltered uraninite from the Cigar Lake deposit, Canada, which has a total oxygen of 2.108 apfu [40]. Relative to the uraninites from the Marshall Pass District, the PbO content of the uraninites from the Happy Jack Mine is low (from 0.72 to 0.81 wt %). The $UO_2$ plus converted radiogenic Pb is from 96.56 to 98.38 wt %. The uraninites also contain some Ca, Zr, Ti, Fe, Si and P (Table 2). The $ThO_2$ content is below detection limits, but the contents of Y and Nd are significant, with approximately 0.28 wt % $Y_2O_3$ and 0.12 wt % $Nd_2O_3$ (Table 2).

*Schoepite*

Schoepite, $[(UO_2)_8O_2(OH)_{12}](H_2O)_{12}$, is a uranyl oxide hydrate, a common alteration product of uraninite. Schoepite was identified in samples from Jefferson County, Colorado (sample # 637), the Marshall Pass District, Colorado (sample # 530 and # 531), and the Happy Jack Mine, Utah (sample # 353) (Table 2). In sample # 637, primary uraninite has altered completely to a suite of secondary uranyl minerals. The bright band of the large concentric structure at the lower left corner of Fig. 2B is strongly dehydrated schoepite, with an average EMPA total close to 100 wt % after converting PbO to $UO_2$ and then $U^{4+}$ to $U^{6+}$. The converted EMPA totals for the inner part of the concentric structure have decreased to 89.32 wt % when close to the center, indicating a high $H_2O$ content, thus a weakly dehydrated schoepite. The schoepite in sample # 637 contains an average of 6.69 wt % PbO, 1.48 wt % $ZrO_2$, 1.05 wt % $TiO_2$, and 0.11 wt % $Y_2O_3$. The Th and other REE contents are below detection limits (Table 2).

Schoepite in samples # 530 and # 531 is closely associated with uraninite. The alternating bright and gray bands in sample # 530 (Fig. 2D) correspond to uraninite and

schoepite, respectively. The gray schoepite bands have a similar chemical composition to the bright uraninite bands, except for the lower $UO_2$ (schoepite 85.41 wt % $UO_2$ and uraninite 89.08 wt % $UO_2$). In sample # 531, a thin schoepite rim (about 10 μm) is located between a massive uraninite core and a late stage uraninite crust. In sample # 353 from the Happy Jack Mine, schoepite has a very low PbO content (0.21 wt %) and an unusually high $TiO_2$ content (1.94 wt %).

*Calciouranoite*

A U- and Ca-rich uranyl phase was found in sample # 369 (Table 2). Besides major components $UO_2$ (82.43 wt %) and CaO (7.14 wt %), the phase also contains significant amounts of $SiO_2$ (1.94 wt %). This phase has a low EMPA total and a U:Ca atomic ratio of 5:2. The low EMPA total suggests that additional components, such as $H_2O$ and $CO_2$, may be present. There are three U- and Ca-dominated uranyl phases: calciouranoite, $(Ca,Ba,Pb)U_2O_7 \cdot 5H_2O$, metacalciouranoite, $(Ca,Na,Ba)U_2O_7 \cdot 2H_2O$, and becquerelite, $Ca(UO_2)_6O_4(OH)_6 \cdot H_2O$. On basis of U:Ca atomic ratio, this phase is closest to calciouranoite or metacalciouranoite. This phase has a low PbO content (0.51 wt %) but has abundant euhedral galena inclusions (Fig. 2F).

*Uranophane*

Uranophane, $Ca(UO_2)_2Si_2O_7 \cdot 6H_2O$, was identified in sample # 637. The phase (bright areas in Fig. 2C) is closely associated with a Fe-rich uranyl phase (gray areas in Fig. 2C; see below) and fills the fractures cutting through the Fe-rich uranyl phase. Besides the major components U, Si and Ca, the uranophane contains low PbO (0.17 wt %) and high $P_2O_5$ (2.23 wt %) and FeO (0.92 wt %). The Th and REE contents are below detection limits (Table 2).

*Fourmarierite*

A Pb-rich uranyl oxide hydrate was identified in sample # 637. The phase contains 11.04 wt % PbO and the U:Pb atomic ratio is 5.6:1, closest to that of fourmarierite, $PbU_4O_{13} \cdot 6H_2O$. Pb-rich curite, $Pb_2U_5O_{17} \cdot 4H_2O$, has a lower U:Pb atomic ratio than the identified phase. The

phase can be easily damaged by the electron beam, therefore, it is probably not the anhydrous Pb-U oxide richetite. The fourmarierite has relatively high $ZrO_2$ (1.25 wt %) and $TiO_2$ (0.89 wt %) contents.

*A Fe-rich uranyl phase*

A Fe-dominated uranyl phase (gray areas in Fig. 2C) was found in sample # 637. Besides major components $UO_2$ (29.27 wt %) and FeO (41.16 wt %), the phase also contains significant amounts of Zr, Ti, Si, Al and Ca (Table 2). The low EMPA total (83.06 wt %) suggests that additional components, such as $H_2O$ and $CO_2$, may be present. Because the common gangue minerals of this sample include ankerite and calcite, the Fe-rich phase is probably a uranyl carbonate.

*Coffinite*

Coffinite, $USiO_4 \cdot nH_2O$, was found in sample # 603. The phase has a U:Si atomic ratio of 1:1 and a low EMPA total of 94.2 wt % (Table 2), neither similar to soddyite $(UO_2)_2SiO_4 \cdot 2H_2O$ (U:Si atomic ratio 2:1) nor to uranophane $Ca(UO_2)_2Si_2O_7 \cdot 6H_2O$ (not enough Ca). This phase is closest to coffinite containing water. The phase contains $Y_2O_3$ as high as 0.9 wt % and $ZrO_2$ is 1.2 wt % (Table 2).

*Variations of chemical compositions*

The chemical compositions of the uranium phases are heterogeneous. EMPA profiles show that compositional zonation exists and that there are correlations between some components. For example in sample # 637 (Fig. 2B), from the rim to the center of a concentric structure, the $UO_2$ and PbO of the schoepite decrease and the $SiO_2$ and CaO increase (Fig. 3). There is a positive correlation between $UO_2$ and $ZrO_2$, and between $UO_2$ and PbO (Fig. 3). However, $SiO_2$ and $TiO_2$ contents apparently decrease with the increase of $UO_2$ (Fig. 3). With increasing alteration, $UO_2$, PbO and $ZrO_2$ decrease from 80.2 to 70.3 wt %, from 6.6 to 0.5 wt %, and from 1.8 to 0.5 wt %, respectively; and $SiO_2$, $TiO_2$, CaO and $P_2O_5$ increase from 0.4 to 6.1

wt %, from 1.1 to 1.8 wt %, from 1.1 to 4.0 wt %, and from 0.3 to 1.2 wt %, respectively. Therefore, alteration processes cause loss of U, Pb and Zr and incorporation of Si, Ti, Ca and P into the schoepite. There are abundant micro-fractures observed in the secondary schoepite from sample # 637 (Fig. 2B). This textural feature, along with compositional variations of the schoepite, suggests that dehydration of schoepite occurred from the rim of the concentric structure and progressed toward the center. The volume decrease associated with dehydration may be responsible for the formation of fractures. Partial dehydration of schoepite was also reported by Finch et al. [43].

In contrast to sample # 637, for sample # 531, the correlation between $UO_2$ and $ZrO_2$ and between $UO_2$ and PbO is negative (Fig. 4). However, there is a positive correlation between $UO_2$ and CaO and between $UO_2$ and $Y_2O_3$ (Fig. 4).

*Trace element contents*

Electron microprobe analyses show that trace element contents of the uraninites and alteration products are low or below the detection limits of the electron microprobe. The highest oxide contents of the uraninites analyzed are $ThO_2$ 0.17, $Y_2O_3$ 0.28, $La_2O_3$ 0.03, $Ce_2O_3$ 0.10, $Pr_2O_3$ 0.02, $Nd_2O_3$ 0.14, $Sm_2O_3$ 0.12, $Eu_2O_3$ 0.04, $Gd_2O_3$ 0.08, $Al_2O_3$ 0.13, $SiO_2$ 0.49, $ZrO_2$ 0.93, and $TiO_2$ 0.54 wt % (Table 2). The highest oxide contents of the uranyl phases analyzed are $ThO_2$ 0.21, $Y_2O_3$ 0.88, $La_2O_3$ 0.05, $Ce_2O_3$ 0.15, $Pr_2O_3$ 0.05, $Nd_2O_3$ 0.18, $Sm_2O_3$ 0.14, $Eu_2O_3$ 0.11, $Gd_2O_3$ 0.08, $Al_2O_3$ 1.25, $ZrO_2$ 2.11, and $TiO_2$ 2.74 wt % (Table 2). Overall, trace element contents of the primary uraninites are lower than those for secondary uranium phases, indicating that secondary phases have a higher capability for incorporating trace elements into their structure than uraninite. This suggests that trace elements do preferentially enter the structures of secondary uranium phases. This conclusion is supported by the compositions of the coexisting uraninite and schoepite from samples # 530 and # 531. In sample # 530, the uraninite has lower $ThO_2$ (0.17 wt %), $SiO_2$ (0.15 wt %), $ZrO_2$ (0.70 wt %) and $TiO_2$ (0.54 wt %) than the coexisting schoepite, which has 0.21 wt % $ThO_2$, 0.16 wt % $SiO_2$, 0.98 wt % $ZrO_2$ and 0.75 wt % $TiO_2$. In

sample # 531, the uraninite has lower $ZrO_2$ (0.37-0.53 wt %), $TiO_2$ (0.20-0.29 wt %), $Y_2O_3$ (0.11-0.14 wt %), $Ce_2O_3$ (0.05-0.10 wt %), $Nd_2O_3$ (0.06-0.14 wt %), $Sm_2O_3$ (0.07-0.12 wt %) and $Eu_2O_3$ (0.01 wt %) than the coexisting schoepite, which has 2.00 wt % $ZrO_2$, 0.42 wt % $TiO_2$, 0.15 wt % $Y_2O_3$, 0.15 wt % $Ce_2O_3$, 0.18 wt % $Nd_2O_3$, 0.14 wt % $Sm_2O_3$ and 0.14 wt % $Eu_2O_3$ (Table 2).

**Conclusions**

1. There are two types of uraninites. One has a high $U^{6+}$ content from 0.587 to 0.808 apfu, close to or similar to altered secondary uraninite with a stoichiometry of $U_3O_8$. The other has a low $U^{6+}$ content from 0.212 to 0.489 apfu, close to that of primary uraninite, such as from the Cigar Lake deposit. Impurity components in uraninites mainly consist of Ca, Zr, Ti, Fe, Si and P. Elements such as Th and REE are low or below the detection limits of the electron microprobe.
2. Schoepite is ubiquitous in the samples analyzed and has two different occurrences. In samples # 530 and # 531, schoepite is closely associated with uraninite, forming alternating bright and gray bands with a concentric structure. In sample # 637, schoepite alone forms the entire concentric structure, with different degrees of dehydration in the different bands. Common minor elements in schoepite are Pb, Zr, and Ti.
3. Compositional zonation of uraninite and uranyl phases is common; and there are correlations between some components. A compositional profile on a concentric structure in schoepite in sample # 637 shows that, with increasing alteration, $UO_2$, PbO and $ZrO_2$ decrease, and $SiO_2$, $TiO_2$, CaO and $P_2O_5$ increase. Alteration causes loss of U, Pb and Zr and incorporation of Si, Ti, Ca and P into uranyl phases.
4. Trace element contents of the uraninites and alteration products are low or below detection limits of electron microprobe. However, the coexisting uraninite and schoepite from samples # 530 and # 531 show that trace element contents of the uraninite are lower than those for

secondary phases. This suggests that some trace elements will preferentially concentrate in the structures of secondary uranium phases during the corrosion of $UO_2$.

5. The formation of secondary uranium minerals is controlled by the interaction between the host rock and primary uranium minerals, for example, Ca-rich calciouranoite or metacalciouranoite formed in limestone, and a Fe-dominated uranyl phase is associated with a Fe carbonate ankerite.
6. Texturally, concentric structures and micro-fractures are common. Concentric structures are usually composed of both uraninite and uranyl phases (e.g., sample # 530 and # 531, Fig. 2D). Micro-fractures, associated with the dehydration of hydrous uranyl phases, are common in secondary phases, e.g., in schoepite from sample # 637 (Fig. 2B).

## Acknowledgements

This study is supported by the Environmental Management Science Program, US Department of Energy through grant # DE-FG07-97-ER14816. The electron microprobe analyzer used in this work was acquired under Grant # EAR-82-12764 from the National Science Foundation. Two anonymous reviewers are thanked for their comments.

## References

1. Ahearne, J.F.: Radioactive waste: the size of the problem. Physics Today 50, 24 (1997).

2. Finch, R.J., Ewing, R.C.: The corrosion of uraninite under oxidizing conditions. J. Nucl. Mat. 190, 133 (1992).

3. Johnson, L.H., Werme, L.O.: Materials characteristics and dissolution behavior of spent nuclear fuel. Mat. Res. Soc. Bulletin 19, 24 (1994).

4. Burns, P.C., Ewing, P.C., Miller, M.L.: Incorporation mechanisms of actinide elements into the structures of $U^{6+}$ phases formed during the oxidation of spent nuclear fuel. J. Nucl. Mat. 245, 1 (1997).

5. Chen, F.R., Burns, P. C., Ewing, P.C.: $^{79}Se$: geochemical and crystallo-chemical retardation mechanisms. J. Nucl. Mat. 275, 81 (1999).

6. Ewing, R.C., Jercinovic, M.J.: Natural analogues: their application to the prediction of the long-term behavior of nuclear waste forms. In: Scientific Basis for Nuclear Waste Management X (J.K. Bates, W.B. Seefeldt, eds.), Proc. Mat. Res. Soc. 84, 67 (1987).

7. Ewing, R.C.: The use of natural systems to predict radionuclide migration. In: Proceedings of the Third International Symposium on Advanced Nuclear Energy Research, Global Environment and Nuclear Energy. Japan Atomic Energy Res. Inst., 167 (1991).

8. Ewing, R.C.: The role of natural analogues in performance assessment: applications and limitations. In: Proceedings of the Third International Conference on High Level Radioactive Waste Management (J.S. Tulenko, ed.). Amer. Nucl. Soc., 1429 (1992).

9. Ewing, R.C.: Long-term predictions using natural analogues. In: Proceedings of symposium sponsored by the Nuclear Regulatory Commission "The Role of Natural Analogs in Geologic Disposal of High-Level Nuclear Waste" (W.M. Murphy, K.A. Kovach, eds.). Center for Nuclear Waste Regulatory Analyses, Report 93-020, 29 (1993).

10. Ewing, R.C.: The long-term performance of nuclear waste forms: the use of natural materials - three case studies. In: Scientific Basis for Nuclear Waste Management XVI (C.G. Interrante, R.T. Pabalan, eds.), Proc. Mat. Res. Soc. 294, 559 (1993).

11. Janeczek, J., Ewing, R.C.: Corrosion and alteration of uraninite under reducing conditions. J. Nucl. Mat. 192, 157 (1992).

12. Janeczek, J., Ewing, R.C.: Mechanisms of lead release from uraninite in the natural fission reactors in Gabon. Geochim. Cosmochim. Acta, 59, 1917 (1995).

13. Janeczek, J., Ewing, R.C., Thomas, L.E.: Oxidation of uraninite: does tetragonal U3O7 occur in nature? J. Nucl. Mat. 207, 176 (1993).

14. Janeczek, J., Ewing, R.C., Oversby, V.M., Werme, L.O.: Uraninite and $UO_2$ in spent nuclear fuel: a comparison. J. Nucl. Mat. 238, 121 (1996).

15. Pearcy, E.C., Prikryl, J.D., Murphy, W.M., Leslie, B.W.: Alteration of uraninite from Nopal I deposit, Peña Blanca District, Chihuahua, Mexico, compared to degradation of spent nuclear fuel in the proposed U.S. high-level nuclear waste repository at Yucca Mountain, Nevada. Applied Geochem. 9, 713 (1994).

16. Pavicevic, M.K., El Goresy, A.: Mineralogy of the uranium deposit of Zirovski Vrh, Slovenia/Yugoslavia: a reflected light, SEM, electron microprobe and PIXE investigation. Monogr. Ser. Min. Dep. 27, 113 (1987).

17. Ruskeeniemi, T., Lindberg, A., Pérez del Villar, L., Blyth, A., Suksi, J., de Pablo, J., Tullborg, E-L.: Uranium mineralogy. In: Abstracts of the 8th EC Natural Analogue Working Group Meeting, Strasbourg, France 1999.

18. Finch, R.J., Ewing, R.C.: Alteration of natural uraninite under oxidizing conditions from Shinkolobwe, Katanga, Zaire: a natural analogue for the corrosion of spent fuel. Radiochim. Acta 52/53, 395 (1991).

19. Jensen, K.A., Ewing, R.C., Gauthier-Lafaye, F.: Uraninite: a 2 Ga spent nuclear fuel from the natural fission reactor at Bangombé in Gabon, West Africa. Mat. Res. Soc. Symp. Proc. Vol. 465, 1209 (1997).

20. Casas, I., Bruno, J., Cera, E., Finch, R.J., Ewing, R.C.: Characterization and dissolution behavior of a becquerelite from Shinkolobwe, Zaire. Geochim. Cosmochim. Acta 61, 3879 (1997).

21. Foord, E.E., Korzeb, S.L., Lichte, F.E., Fitzpatrick, J.J.: Additional studies on mixed uranyl oxide-hydroxide hydrate alteration products of uraninite from the Palermo and Ruggles granitic pegmatites, Grafton County, New Hampshire. Can. Min. 35, 145 (1997).

22. Forster, H.J.: The chemical composition of uraninite in Variscan granites of the Erzgebirge, Germany. Min. Mag. 63, 239 (1999).

23. Jensen, K.A., Ewing, R.C.: Microtexture and chemistry of "unaltered" uraninite in the Oklo, Okélobondo, and Bangombé Natural Fission Reactors. In: Proceedings of the 2nd Oklo Phase II Workshop, Nuclear Science and Technology (Louvat, D., Michaud, V., and von arevic, H., eds.). EUR 19116 EN, 61-91

24. Bruno, J., Casas, I., Duro, L., Pérez, I., Pérez del Villar, L.: Spent fuel studies in the Oklo natural analogue. In: Abstracts of the 8th EC Natural Analogue Working Group Meeting, Strasbourg, France (1999).

25. Pagel, M., Pinte, G., Rotach-Toulhoat, N.: The rare earth elements in natural uranium oxides. Monogr. Ser. Min. Dep. 27, 81 (1987).

26. Zetterström, L.: SIMS studies on uraninite from Oklo, Gabon. In: Abstracts of European Union of Geosciences (EUG 10), Strasbourg, France, p. 524 (1999).

27. Bastin, G.F., van Voo, F.J.J., Heijligers, H.J.M.: Evaluation and use of Gaussian $\phi(\rho z)$ curves in quantitative electron probe microanalysis: a new optimization. X-ray Spectrum 13, 91 (1984).

28. Patterson, J.A.: Character of the United States uranium resources. In: Uranium Exploration Geology, p. 117. International Atomic Energy Agency, Vienna 1970.

29. Rick, R.A., Holland, H.D., Peterson, U.: Hydrothermal Uranium Deposits, Developments in Economic Geology 6, Elsevier, Amsterdam 1977, 264 p.

30. Bowie, S.H.U.: World uranium deposits. In: Uranium Exploration Geology, p. 23. Int. Atomic Energy Agency, Vienna 1970.

31. Gruner, J.W., Feltzer, W.G., Rapaport, I.: The uranium deposits near Marysvale, Piute County, Utah. Econ. Geol. 46, 243 (1951).

32. Drake, Jr., A.A.: Geology of the Wood and East Calhoun Mines Central City District, Gilpin County, Colorado. U. S. Geol. Surv. Bull. 1032-C, 129 (1957).

33. Walker, G.W., Osterwald, F.W., Adams, J.W.: Geology of uranium-bearing veins in the conterminous United States. U. S. Geol. Surv. Prof. Pap. 455 (1963).

34. Sheridan, D.M., Maxwell, C.H., Albee, A.L.: Geology and uranium deposits of the Ralston Buttes district, Jefferson County, Colorado. U. S. Geol. Surv. Prof. Pap. 520 (1967).

35. Ludwig, K.R., Wallace, A.R., Simmons, K.R.: The Schwartzwalder uranium deposit; II, Age of uranium mineralization and lead isotope constraints on genesis. Econ. Geol. 80, 1858 (1985).

36. Olson, J.C.: Geology and uranium deposits of the Cochetopa and Marshall Pass districts, Saguache and Gunnison counties, Colorado. U. S. Geological Survey Professional Paper 1457, 44 p (1988).

37. Dahlkamp, F.J.: Uranium Ore Deposits. Springer-Verlag, Berlin 1993, 460 p.

38. Ludwig, K.R., Simmons, K.R., Webster, J.D.: U-Pb isotope systematics and apparent ages of uranium ores, Ambrosia Lake and Smith Lake districts, Grant mineral belt, New Mexico. Econ. Geol. 79, 322 (1984).

39. Finch, R.J., Cooper, M.A., Hawthorne, F.C., Ewing, R.C.: The crystal structure of schoepite, $[(UO_2)_8O_2(OH)_{12}](H_2O)_{12}$. Can. Min. 34, 1071 (1996).

40. Janeczek, J., Ewing, R.C.: The structural formula of uraninite. J. Nucl. Mat. 190, 128 (1992).

41. Janeczek, J., Ewing, R.C., Thomas, L.E.: Oxidation of uraninite: Does tetragonal $U_3O_7$ occur in nature? J. Nucl. Mat. 207, 176 (1993).

42. Fayek, M., Kyser, T.K.: Characterization of multiple fluid events and rare earth mobility associated with formation of unconformity-type uranium deposits in the Athabasca Basin, Saskatchewan. Can. Min. 35, 627 (1997).

43. Finch, R.J., Miller, M.L., Ewing, R.C.: Weathering of natural uranyl oxide hydrates: Schoepite polytypes and dehydration effects. Radiochim. Acta 58/59, 433 (1992).

## Tables

Table 1. EMPA procedure for the analysis of natural uraninite $UO_{2+x}$ and its alteration products

| Element | X-ray | Crystal | Beam | Standard: formula/name (weight fraction) |
|---|---|---|---|---|
| Na | $K_\alpha$ | TAP | 20 nA | $NaAlSi_3O_8$/TAB (Na 0.0876, Al 0.1029, Si 0.3213, O 0.4882) |
| Mg | $K_\alpha$ | TAP | 20 nA | $(Mg,Fe)_2SiO_4$/MARJ (Mg 0.2899, Fe 0.0897, Mn 0.0022, Si 0.1881, Cr 0.0005, O 0.4333) |
| Al | $K_\alpha$ | TAP | 20 nA | $Al_2SiO_5$/ANDA (Al 0.3331, Si 0.1734, O 0.4935) |
| Si | $K_\alpha$ | TAP | 20 nA | $Al_2SiO_5$/ANDA (Al 0.3331, Si 0.1734, O 0.4935) |
| P | $K_\alpha$ | TAP | 20 nA | $YPO_4$/YPO (P 0.1648, Y 0.4835, O 0.3481) |
| K | $K_\alpha$ | PET | 20 nA | $KAlSi_3O_8$/ GKFS (K 0.1234, Al 0.1016, Fe 0.0006, Mg 0.0006, Ba 0.0010, Ca 0.0008, Na 0.0103, Si 0.3005, O 0.4611) |
| Ca | $K_\alpha$ | PET | 20 nA | $CaWO_4$/SCHL (Ca 0.1392, W 0.6385, O 0.2222) |
| La | $L_\alpha$ | PET | 20 nA | $LaPO_4$/LAPO (La 0.5862, P 0.1307, Pb 0.0104, O 0.2717) |
| Ce | $L_\alpha$ | PET | 20 nA | $CePO_4$/CEPO (Ce 0.5857, P 0.1295, Pb 0.0166, O 0.2701) |
| U | $M_\beta$ | PET | 80 nA | $UO_2$/URAN (U 0.8810, O 0.1190) |
| Th | $M_\alpha$ | PET | 80 nA | THOR (Th 0.6257 U 0.2233 Pb 0.0320 O 0.1190) |
| S | $K_\alpha$ | PET | 20 nA | PbS/PBS (S 0.1340, Pb 0.8660) |
| Sr | $L_\alpha$ | PET | 20 nA | $SrSO_4$/CELE (Sr 0.4770, S 0.1750, O 0.3480) |
| Y | $L_\alpha$ | PET | 20 nA | $YPO_4$/YPO (P 0.1648, Y 0.4835, O 0.3481) |
| Zr | $L_\alpha$ | PET | 20 nA | $ZrSiO_4$/ZIRC (Zr 0.4980, Si 0.1530, O 0.3490) |
| Pb | $M_\alpha$ | PET | 80 nA | PbS/PBS (S 0.1340, Pb 0.8660) |
| Mn | $K_\alpha$ | PET | 20 nA | $MnSiO_3$/BHRH (Mn 0.2927, Al 0.0004, Fe 0.1210, Si 0.2138, Mg 0.0004, Ca 0.0094, Na 0.0009, K 0.0002, O 0.3564) |
| Ti | $K_\alpha$ | LiF | 20 nA | $FeTiO_3$/ILM (Ti 0.3049, Mg 0.0770, Mn 0.0024, Cr 0.0078, Fe 0.2624, O 0.3473) |
| Fe | $K_\alpha$ | LiF | 20 nA | $Fe_3Al_2Si_3O_{12}$/IALM (Fe 0.2446, Ti 0.0015, Al 0.1074, Si 0.1754, Mg 0.0083, Mn 0.0137, Ca 0.0529, Na 0.0009, K 0.0003, O 0.3959) |
| Pr | $L_\alpha$ | LiF | 20 nA | $PrPO_4$/PRPO (Pr 0.5932, P 0.1304, Pb 0.0083, O 0.2707) |
| Nd | $L_\alpha$ | LiF | 20 nA | $NdPO_4$/NDPO (Nd 0.5972, P 0.1282, Pb 0.0083, O 0.2675) |
| Sm | $L_\alpha$ | LiF | 20 nA | $SmPO_4$/SMPO (Sm 0.6074, P 0.1251, Pb 0.0070, O 0.2609) |
| Eu | $L_\alpha$ | LiF | 20 nA | $EuPO_4$/EUPO (Eu 0.6154, P 0.1254, O 0.2592) |
| Gd | $L_\alpha$ | LiF | 20 nA | $GdPO_4$/GDPO (Gd 0.6234, P 0.1228, O 0.2538) |

Notes: Accelerating voltage 20 kV. Peak count time 30 seconds. $M_\beta$ was used for U to avoid interference from Th $L_\gamma$, Zr $K_\alpha$, Fe $K_\alpha$ and Pb $L_\beta$ lines.

Table 2. Electron microprobe analyses of uranium minerals

| Sample # | 603 | 637 | 637 | 637 | 637 | 530 | 530 |
|---|---|---|---|---|---|---|---|
| Phase | Coffinite | Schoepite | Fe-rich phase | Uranophane | Fourmarierite | Uraninite (bright) | Schoepite (gray) |
| Analyses # | 16 | 4 | 4 | 3 | 2 | 6 | 6 |
| $UO_2$ | 70.85 | 81.21 | 29.27 | 69.45 | 77.04 | 89.08 | 85.41 |
| $ThO_2$ | 0.13 | 0.09 | 0.18 | 0.02 | 0.07 | 0.17 | 0.21 |
| $SiO_2$ | 16.02 | 0.38 | 2.57 | 11.36 | 0.32 | 0.15 | 0.16 |
| $TiO_2$ | 0.07 | 1.05 | 2.74 | 0.11 | 0.89 | 0.54 | 0.75 |
| $ZrO_2$ | 1.23 | 1.48 | 2.11 | 0.03 | 1.25 | 0.70 | 0.98 |
| PbO | 0.06 | 6.69 | 1.73 | 0.17 | 11.04 | 1.58 | 1.44 |
| MnO | 0.13 | 0.13 | 0.10 | 0.00 | 0.10 | 0.03 | 0.04 |
| FeO | 0.30 | 0.20 | 41.16 | 0.92 | 0.16 | 0.31 | 0.27 |
| MgO | 0.01 | 0.01 | 0.00 | 0.00 | 0.01 | 0.01 | 0.01 |
| CaO | 1.83 | 1.09 | 0.95 | 5.98 | 0.81 | 1.48 | 1.41 |
| SrO | 0.00 | 0.01 | 0.05 | 0.01 | 0.00 | 0.01 | 0.01 |
| $Na_2O$ | | | | | | | |
| $K_2O$ | | | | | | | |
| $Al_2O_3$ | 0.71 | 0.08 | 1.25 | 0.05 | 0.09 | 0.07 | 0.08 |
| $P_2O_5$ | 1.21 | 0.32 | 0.74 | 2.23 | 0.46 | 0.14 | 0.13 |
| $SO_3$ | 0.46 | 0.02 | 0.06 | 0.01 | 0.05 | 0.03 | 0.03 |
| $Y_2O_3$ | 0.88 | 0.11 | 0.08 | 0.00 | 0.07 | 0.09 | 0.08 |
| $La_2O_3$ | 0.05 | 0.01 | 0.01 | 0.00 | 0.03 | 0.03 | 0.03 |
| $Ce_2O_3$ | 0.08 | 0.00 | 0.00 | 0.00 | 0.00 | 0.00 | 0.02 |
| $Pr_2O_3$ | 0.01 | 0.01 | 0.00 | 0.00 | 0.05 | 0.01 | 0.00 |
| $Nd_2O_3$ | 0.04 | 0.04 | 0.01 | 0.00 | 0.00 | 0.03 | 0.06 |
| $Sm_2O_3$ | 0.06 | 0.02 | 0.02 | 0.01 | 0.04 | 0.08 | 0.03 |
| $Eu_2O_3$ | 0.02 | 0.00 | 0.00 | 0.03 | 0.00 | 0.03 | 0.03 |
| $Gd_2O_3$ | 0.06 | 0.04 | 0.02 | 0.03 | 0.04 | 0.05 | 0.07 |
| Σ1 | 94.19 | 92.98 | 83.06 | 90.41 | 92.54 | 94.63 | 91.24 |
| $UO_2$(+Pb) | 70.92 | 89.30 | 31.36 | 69.65 | 90.41 | 90.99 | 87.15 |
| Σ2 | 94.20 | 94.38 | 83.42 | 90.45 | 94.86 | 94.96 | 91.54 |
| $UO_2$ | 0.00 | 0.00 | 0.00 | 0.00 | 3.58 | 5.91 | 0.00 |
| $UO_3$ | 75.12 | 94.59 | 33.22 | 73.78 | 91.98 | 90.13 | 92.31 |
| Σ3 | 98.41 | 99.68 | 85.28 | 94.58 | 100.00 | 100.00 | 96.70 |
| 1 cation | | | | | | | |
| U(total) | 0.420 | 0.838 | 0.138 | 0.429 | 0.857 | 0.864 | 0.851 |
| Th | 0.001 | 0.001 | 0.001 | 0.000 | 0.001 | 0.002 | 0.002 |
| Si | 0.426 | 0.016 | 0.051 | 0.314 | 0.013 | 0.007 | 0.007 |
| Ti | 0.001 | 0.033 | 0.041 | 0.002 | 0.029 | 0.017 | 0.025 |
| Zr | 0.016 | 0.030 | 0.020 | 0.000 | 0.026 | 0.015 | 0.021 |
| Mn | 0.003 | 0.005 | 0.002 | 0.000 | 0.004 | 0.001 | 0.001 |
| Fe | 0.007 | 0.007 | 0.682 | 0.021 | 0.006 | 0.011 | 0.010 |
| Mg | 0.001 | 0.001 | 0.000 | 0.000 | 0.001 | 0.000 | 0.000 |
| Ca | 0.052 | 0.049 | 0.020 | 0.177 | 0.037 | 0.067 | 0.066 |
| Sr | 0.000 | 0.000 | 0.001 | 0.000 | 0.000 | 0.000 | 0.000 |
| Na | 0.000 | 0.000 | 0.000 | 0.000 | 0.000 | 0.000 | 0.000 |
| K | 0.000 | 0.000 | 0.000 | 0.000 | 0.000 | 0.000 | 0.000 |
| Al | 0.022 | 0.004 | 0.029 | 0.002 | 0.005 | 0.003 | 0.004 |
| P | 0.027 | 0.011 | 0.012 | 0.052 | 0.016 | 0.005 | 0.005 |
| S | 0.009 | 0.001 | 0.001 | 0.000 | 0.002 | 0.001 | 0.001 |
| Y | 0.012 | 0.003 | 0.001 | 0.000 | 0.002 | 0.002 | 0.002 |
| La | 0.000 | 0.000 | 0.000 | 0.000 | 0.000 | 0.000 | 0.001 |
| Ce | 0.001 | 0.000 | 0.000 | 0.000 | 0.000 | 0.000 | 0.000 |
| Pr | 0.000 | 0.000 | 0.000 | 0.000 | 0.001 | 0.000 | 0.000 |
| Nd | 0.000 | 0.001 | 0.000 | 0.000 | 0.000 | 0.000 | 0.001 |
| Sm | 0.001 | 0.000 | 0.000 | 0.000 | 0.001 | 0.001 | 0.001 |
| Eu | 0.000 | 0.000 | 0.000 | 0.000 | 0.000 | 0.000 | 0.000 |
| Gd | 0.001 | 0.001 | 0.000 | 0.000 | 0.001 | 0.001 | 0.001 |
| Σcation | 1.000 | 1.000 | 1.000 | 1.000 | 1.000 | 1.000 | 1.000 |
| ΣO | 1.942 | 1.941 | 1.287 | 1.826 | 1.959 | 1.918 | 1.920 |
| $U^{4+}$ | 0.000 | 0.000 | 0.000 | 0.000 | 0.034 | 0.056 | 0.000 |
| $U^{6+}$ | 0.420 | 0.838 | 0.138 | 0.429 | 0.823 | 0.808 | 0.851 |
| ΣO | 2.361 | 2.778 | 1.425 | 2.255 | 2.782 | 2.727 | 2.772 |

Σ1 all oxides from EMPA, Σ2 after PbO converted to $UO_2$, Σ3 after $UO_2$ recalculated into $UO_2$ and $UO_3$. 603: Caribou, Colorado, gneiss host rock; 637: Jefferson, Colorado, metasedimentary rock; 530 and 531: Marshall Pass, Colorado, limestone.

Table 2. Electron microprobe analyses of uranium minerals (continued)

| Sample # | 531 | 531 | 531 | 353 | 386 | 393 | 369 |
|---|---|---|---|---|---|---|---|
| Phase | Uraninite (central) | Schoepite (gray edge) | Uraninite (bright crust) | Schoepite | Uraninite | Uraninite | Calciouranoite |
| Analyses # | 5 | 3 | 4 | 4 | 7 | 43 | 28 |
| $UO_2$ | 88.99 | 82.35 | 90.41 | 86.23 | 90.18 | 91.50 | 82.43 |
| $ThO_2$ | 0.04 | 0.01 | 0.04 | 0.03 | 0.02 | 0.02 | 0.01 |
| $SiO_2$ | 0.11 | 0.00 | 0.13 | 0.33 | 0.49 | 0.46 | 1.94 |
| $TiO_2$ | 0.29 | 0.42 | 0.20 | 1.94 | 0.34 | 0.17 | 0.03 |
| $ZrO_2$ | 0.37 | 2.00 | 0.53 | 0.37 | 0.63 | 0.93 | 0.04 |
| PbO | 2.51 | 2.59 | 1.53 | 0.21 | 0.72 | 0.81 | 0.51 |
| MnO | 0.06 | 0.01 | 0.05 | 0.11 | 0.05 | 0.06 | 0.21 |
| FeO | 0.24 | 0.16 | 0.28 | 0.15 | 0.61 | 0.65 | 0.01 |
| MgO | 0.01 | 0.00 | 0.00 | 0.01 | 0.01 | 0.01 | 0.02 |
| CaO | 1.41 | 1.37 | 2.04 | 1.03 | 2.65 | 2.31 | 7.14 |
| SrO | 0.00 | 0.00 | 0.01 | 0.01 | 0.02 | 0.02 | 0.06 |
| $Na_2O$ | | | | 0.16 | | | 0.23 |
| $K_2O$ | | | | 0.10 | | | 0.27 |
| $Al_2O_3$ | 0.13 | 0.26 | 0.13 | 0.63 | 0.02 | 0.04 | 0.14 |
| $P_2O_5$ | 0.10 | 0.13 | 0.14 | 0.96 | 0.28 | 0.24 | 0.22 |
| $SO_3$ | 0.01 | 0.02 | 0.01 | 0.85 | 0.02 | 0.58 | 0.16 |
| $Y_2O_3$ | 0.11 | 0.15 | 0.14 | 0.14 | 0.28 | 0.27 | 0.02 |
| $La_2O_3$ | 0.02 | 0.03 | 0.03 | 0.01 | 0.01 | 0.02 | 0.01 |
| $Ce_2O_3$ | 0.10 | 0.15 | 0.05 | 0.00 | 0.00 | 0.00 | 0.00 |
| $Pr_2O_3$ | 0.02 | 0.01 | 0.01 | 0.01 | 0.01 | 0.00 | 0.00 |
| $Nd_2O_3$ | 0.14 | 0.18 | 0.06 | 0.07 | 0.10 | 0.14 | 0.01 |
| $Sm_2O_3$ | 0.12 | 0.14 | 0.07 | 0.04 | 0.05 | 0.07 | 0.02 |
| $Eu_2O_3$ | 0.01 | 0.11 | 0.01 | 0.00 | 0.04 | 0.03 | 0.00 |
| $Gd_2O_3$ | 0.08 | 0.08 | 0.08 | 0.08 | 0.03 | 0.06 | 0.02 |
| Σ1 | 94.85 | 90.20 | 95.93 | 93.46 | 96.56 | 98.38 | 93.49 |
| $UO_2$(+Pb) | 92.03 | 85.49 | 92.25 | 86.48 | 91.05 | 92.49 | 83.04 |
| Σ2 | 95.38 | 90.75 | 96.25 | 93.50 | 96.71 | 98.55 | 93.60 |
| $UO_2$ | 14.05 | 0.00 | 28.96 | 0.00 | 35.58 | 68.07 | 0.00 |
| $UO_3$ | 82.59 | 90.55 | 67.05 | 91.61 | 58.75 | 25.86 | 87.96 |
| Σ3 | 100.00 | 95.81 | 100.00 | 98.63 | 100.00 | 100.00 | 98.52 |
| 1 cation | | | | | | | |
| U(total) | 0.881 | 0.838 | 0.855 | 0.760 | 0.802 | 0.802 | 0.623 |
| Th | 0.000 | 0.000 | 0.000 | 0.000 | 0.000 | 0.000 | 0.000 |
| Si | 0.005 | 0.000 | 0.006 | 0.013 | 0.020 | 0.018 | 0.065 |
| Ti | 0.009 | 0.014 | 0.006 | 0.058 | 0.010 | 0.005 | 0.001 |
| Zr | 0.008 | 0.043 | 0.011 | 0.007 | 0.012 | 0.018 | 0.001 |
| Mn | 0.002 | 0.000 | 0.002 | 0.004 | 0.002 | 0.002 | 0.006 |
| Fe | 0.008 | 0.006 | 0.010 | 0.005 | 0.020 | 0.021 | 0.000 |
| Mg | 0.001 | 0.000 | 0.000 | 0.000 | 0.000 | 0.000 | 0.001 |
| Ca | 0.065 | 0.065 | 0.091 | 0.044 | 0.112 | 0.096 | 0.258 |
| Sr | 0.000 | 0.000 | 0.000 | 0.000 | 0.000 | 0.000 | 0.001 |
| Na | 0.000 | 0.000 | 0.000 | 0.012 | 0.000 | 0.000 | 0.015 |
| K | 0.000 | 0.000 | 0.000 | 0.005 | 0.000 | 0.000 | 0.012 |
| Al | 0.006 | 0.014 | 0.006 | 0.029 | 0.001 | 0.002 | 0.005 |
| P | 0.003 | 0.005 | 0.005 | 0.032 | 0.009 | 0.008 | 0.006 |
| S | 0.000 | 0.001 | 0.000 | 0.025 | 0.001 | 0.017 | 0.004 |
| Y | 0.002 | 0.004 | 0.003 | 0.003 | 0.006 | 0.006 | 0.000 |
| La | 0.000 | 0.001 | 0.000 | 0.000 | 0.000 | 0.000 | 0.000 |
| Ce | 0.002 | 0.002 | 0.001 | 0.000 | 0.000 | 0.000 | 0.000 |
| Pr | 0.000 | 0.000 | 0.000 | 0.000 | 0.000 | 0.000 | 0.000 |
| Nd | 0.002 | 0.003 | 0.001 | 0.001 | 0.001 | 0.002 | 0.000 |
| Sm | 0.002 | 0.002 | 0.001 | 0.001 | 0.001 | 0.001 | 0.000 |
| Eu | 0.000 | 0.002 | 0.000 | 0.000 | 0.000 | 0.000 | 0.000 |
| Gd | 0.001 | 0.001 | 0.001 | 0.001 | 0.000 | 0.001 | 0.000 |
| Σcation | 1.000 | 1.000 | 1.000 | 1.000 | 1.000 | 1.000 | 1.000 |
| ΣO | 1.918 | 1.918 | 1.893 | 1.946 | 1.865 | 1.895 | 1.697 |
| $U^{4+}$ | 0.135 | 0.000 | 0.268 | 0.000 | 0.314 | 0.591 | 0.000 |
| $U^{6+}$ | 0.747 | 0.838 | 0.587 | 0.760 | 0.489 | 0.212 | 0.623 |
| ΣO | 2.664 | 2.756 | 2.480 | 2.706 | 2.354 | 2.107 | 2.321 |

353, 386 and 393: Happy Jack, Utah, quartz sandstone; 369: Grants, New Mexico, limestone.

**Figure Captions**

Fig. 1. Map of the Four Corners area of western United States showing localities of uranium minerals studied. 1. Caribou Mine, Boulder County, Colorado; 2. Jefferson County, Colorado; 3. Marshall Pass District, Saguache County, 4. Colorado; Happy Jack Mine, White Canyon, near Blanding, Utah; and 5. Grants, New Mexico.

Fig. 2. Backscattered electron images of uraninite-bearing samples from the Colorado Plateau. (A) Concentric structure; subhedral and anhedral galenas closely associated with uranium minerals (sample # 603). (B) Concentric structure of uranium minerals (sample # 637). (C) Coexisting uranium minerals in sample # 637: uranophane in the bright areas, an Fe-rich uranyl phase in the gray areas, and the dark K-feldspar. (D) Concentric structure of uraninite and schoepite (sample # 530). (E) Anhedral uraninites (bright areas) along the bedding of rounded quartz grains (dark areas) in quartz sandstone (sample # 386). (F) Galena inclusions in calciouranoite (sample # 369).

Fig. 3. Compositional variation of schoepite from the rim (0 μm) to the center (300 μm) of a concentric structure in sample # 637 (Fig. 2B) and the correlation between $UO_2$ and other components.

Fig. 4. Correlation between $UO_2$ and other components for uranium phases in sample # 531.

Fig. 1

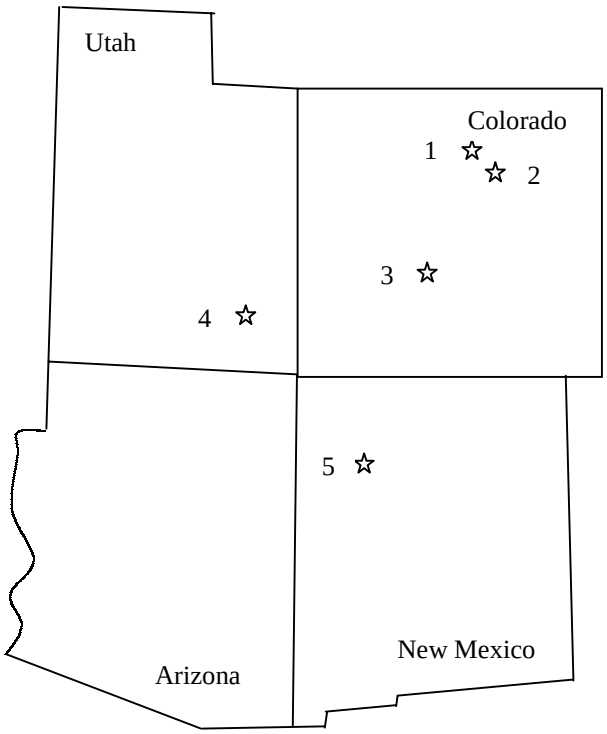

Fig. 2.

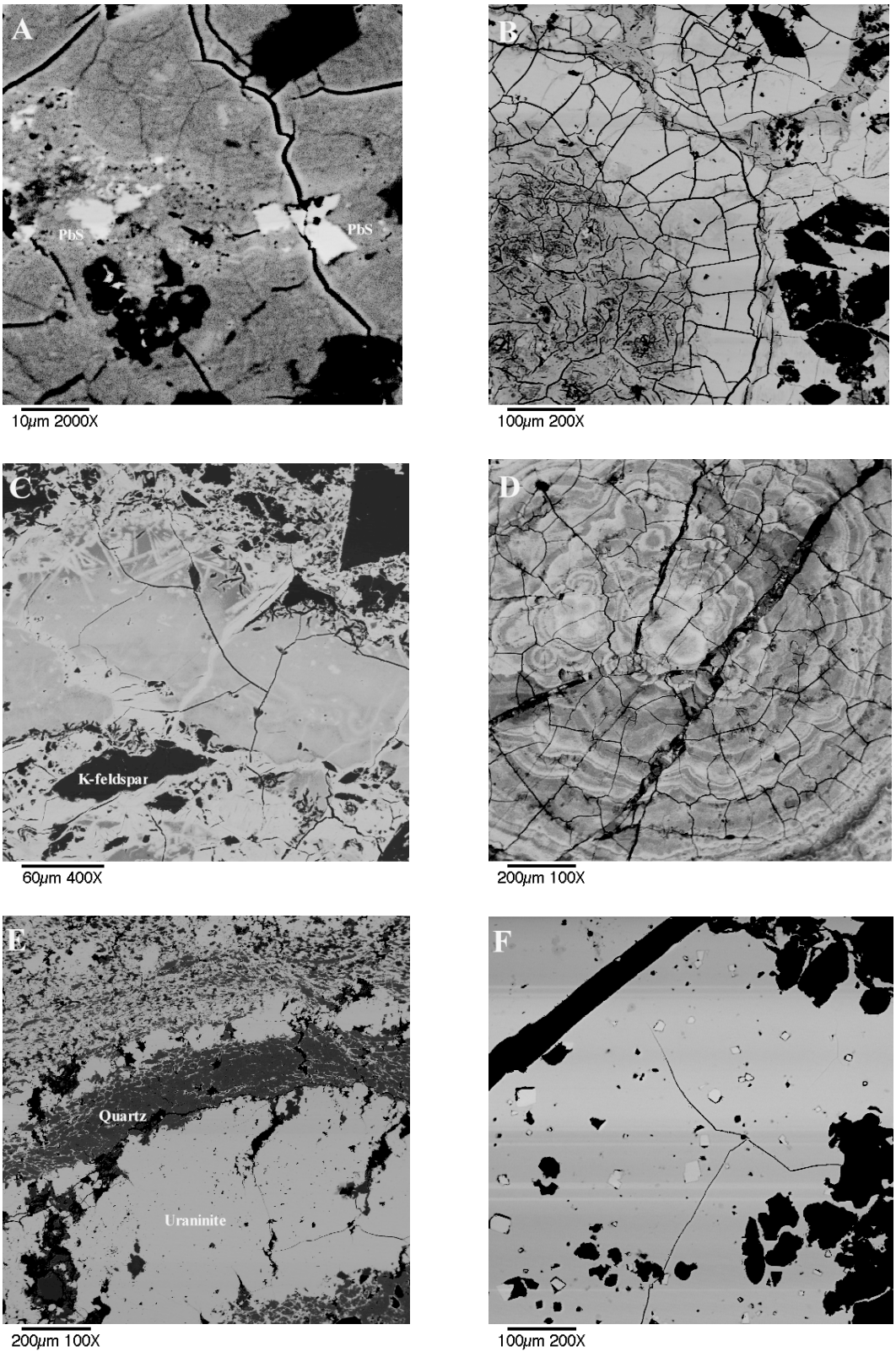
A
PbS
PbS
10μm 2000X
B
100μm 200X
C
K-feldspar
60μm 400X
D
200μm 100X
E
Quartz
Uraninite
200μm 100X
F
100μm 200X

Fig. 3

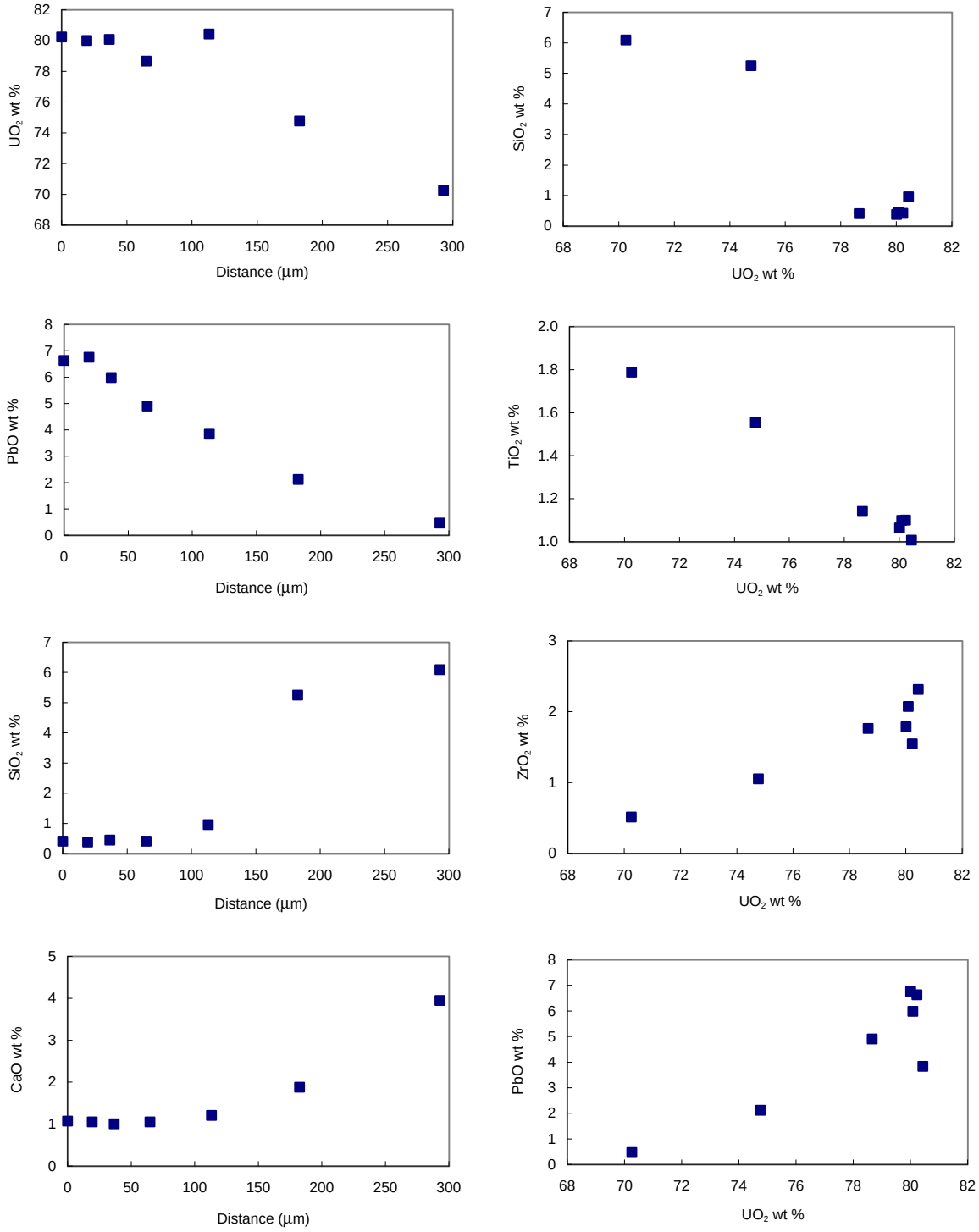
UO2 wt %
Distance (µm)
SiO2 wt %
UO2 wt %
PbO wt %
Distance (µm)
TiO2 wt %
UO2 wt %
SiO2 wt %
Distance (µm)
ZrO2 wt %
UO2 wt %
CaO wt %
Distance (µm)
PbO wt %
UO2 wt %

Fig. 4

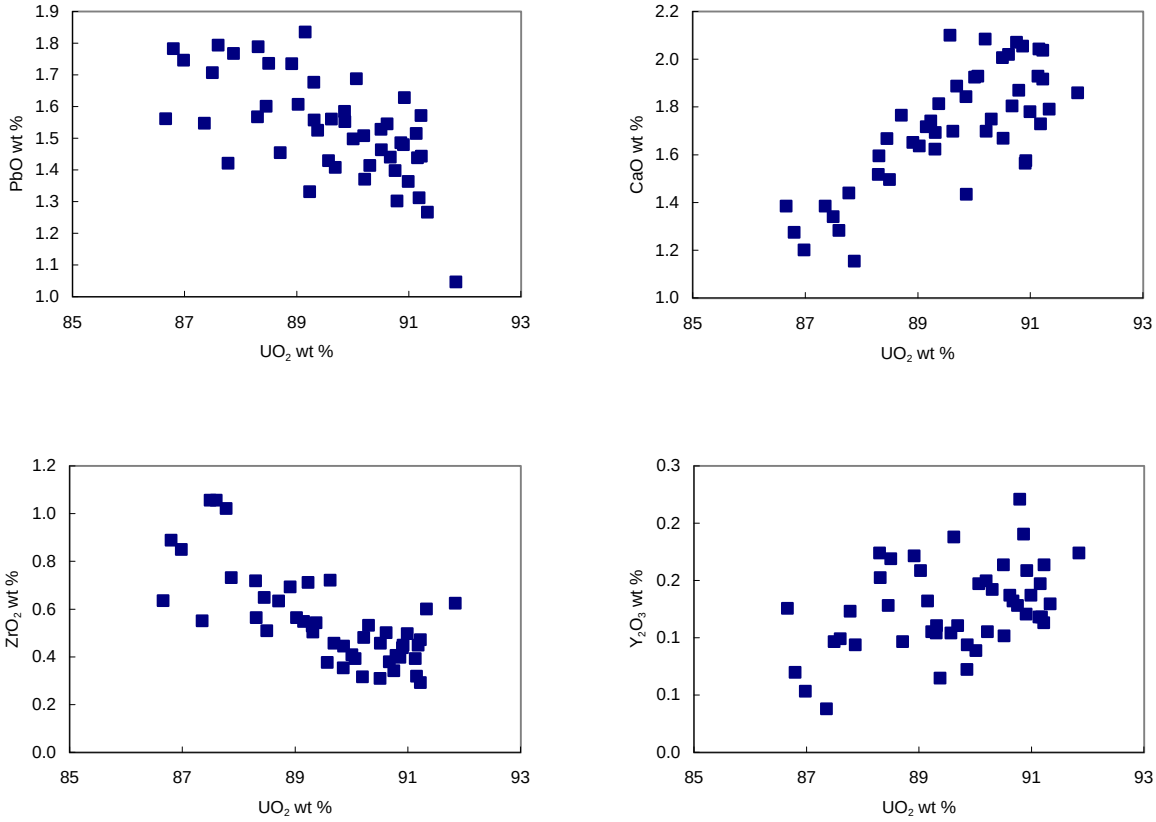
PbO wt %
1.9
1.8
1.7
1.6
1.5
1.4
1.3
1.2
1.1
1.0
85
87
89
91
93
UO2 wt %
CaO wt %
2.2
2.0
1.8
1.6
1.4
1.2
1.0
85
87
89
91
93
UO2 wt %
ZrO2 wt %
1.2
1.0
0.8
0.6
0.4
0.2
0.0
85
87
89
91
93
UO2 wt %
Y2O3 wt %
0.3
0.2
0.2
0.1
0.1
0.0
85
87
89
91
93
UO2 wt %